JACS
JOURNAL OF THE AMERICAN CHEMICAL SOCIETY
Article
pubs.acs.org/JACS

Metal Thiophosphates with Good Mid-infrared Nonlinear Optical Performances: A First-Principles Prediction and Analysis

Lei Kang,[†,‡] Molin Zhou,[†,‡] Jiyong Yao,[†] Zheshuai Lin,[*,†] Yicheng Wu,[†] and Chuangtian Chen[†]

[†]Center for Crystal R&D, Key Lab of Functional Crystals and Laser Technology of Chinese Academy of Sciences, Technical Institute of Physics and Chemistry, Chinese Academy of Sciences, Beijing 100190, PR China

[‡]University of Chinese Academy of Sciences, Beijing 100190, PR China

Supporting Information

ABSTRACT: The family of metal thiophosphates is an important but long-ignored compound system of the nonlinear optical (NLO) materials with desirable properties for the mid-infrared (mid-IR) coherent light generation. In the present work, the mid-IR NLO capabilities of metal thiophosphate crystals are systematically investigated based on their structure−property relationship. The linear and nonlinear optical properties of these crystals are predicted and analyzed using the first-principles calculations. In particular, several metal thiophosphate compounds are highlighted to exhibit good mid-IR NLO performances, as supported by the primary experimental results. These candidates would greatly promote the development of the mid-IR NLO functional materials.

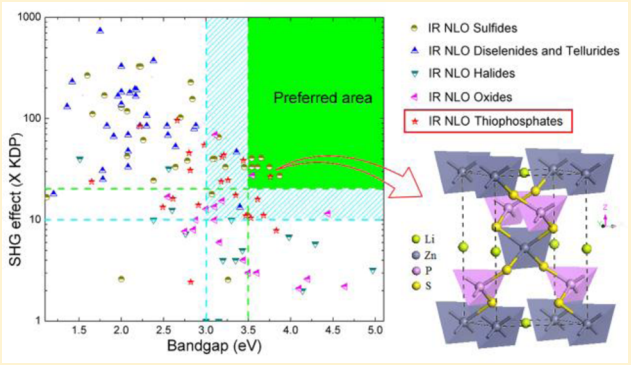

1. INTRODUCTION

Nonlinear optical (NLO) crystals are of great importance for frequency conversion to produce new coherent light sources with tunable frequencies where ordinary lasers perform poorly.[1,2] Numerous NLO materials such as KH_2PO_4 (KDP),[3] $KTiOPO_4$ (KTP),[4] β-BaB_2O_4 (BBO),[5] LiB_3O_5 (LBO),[6] and $LiNbO_3$ (LN)[7] were discovered, and have been widely applied in the spectral regions from ultraviolet (UV) to near-infrared (IR) across the wavelength range of 0.2−2 μm. However, commercially available laser sources with reasonable efficiency are still very limited in the deep-UV (<200 nm) and mid/far-IR (>2 μm) regions, which are confronted by various fundamental challenges and strongly impacted by the availability of enabling NLO materials.[8] With the development of advanced materials science, the deep-UV "200 nm wall" has been broken by the $KBe_2BO_3F_2$ (KBBF) crystal recently,[9,10] but the search of good NLO crystals for mid/far-IR lasers, e.g., in the so-called "fingerprint" region for organic−inorganic molecules, is difficult as before.[11] Therefore, the promising mid/far-IR NLO materials are urgently demanded. In this work, the potential NLO materials applied in the mid-IR region (2−8 μm) will be focused on.

In general, practically usable mid-IR NLO materials should satisfy the following conditions for optical performances: (I) Good IR transparency particularly in the important mid-IR atmospheric window (3−5 μm). It is known that chalcogenides have better transparency in this spectral region of interest compared with oxides or organic materials. Thus, they have been attracted significant attentions for the pursuit of new mid-IR NLO materials.[11] (II) Large second harmonic generation (SHG) coefficient d_{ij}. In order to obtain the high NLO conversion efficiency, empirically, the SHG effect for a mid-IR NLO crystal should be at least 10 times (preferably 20 times) larger than that of KDP (d_{36} = 0.39 pm/V).[12] Accordingly, the optically active structural units with large microscopic second-order susceptibilities should be preferentially arranged in an additive manner in crystal. These microscopic structural units usually include polar chalcogenide units, second-order Jahn−Teller (SOJT) distorted octahedra,[13] or stereochemically active lone electron pairs (SALP) cations.[14] (III) High laser damage threshold (LDT). Essentially, the LDT strongly depends on the bandgap E_g in crystal. For a good mid-IR NLO crystal the E_g should be at least more than 3.0 eV (preferably beyond 3.5 eV), which is enough for most of academic and commercial purposes.[12,15] (IV) Good IR phase-matchability, practically requesting a moderate optical birefringence. The small birefringence (e.g., Δn < 0.04) would not be suitable to achieve the phase-matching condition in the mid-IR region, while the too large birefringence (e.g., Δn > 0.10) would result in the destructive optical behaviors such as self-focus and walk-off effects in the conversion process. Preferably, the birefringence for a good mid-IR material should be in the range of 0.04−0.10. In addition, the good chemical stability and mechanical property are very beneficial to the practical applications of a NLO crystal.

Note that an increase of E_g (corresponding to the blue-shift of short-wave absorption edge λ_{cutoff}) would always result in a decrease of d_{ij} in the NLO crystal. Consequently, to achieve a

Received: July 28, 2015
Published: September 23, 2015

DOI: 10.1021/jacs.5b07920
J. Am. Chem. Soc. 2015, 137, 13049−13059

good performance of the mid-IR NLO crystal the balance between the conditions (II) and (III) (i.e., d_{ij} vs E_g) must be significantly focused on. Namely, the elementary balance for a good mid-IR NLO crystal should be $d_{ij} > 10 \times$ KDP and $E_g > 3.0$ eV, while the preferred balance should be $d_{ij} > 20 \times$ KDP and $E_g > 3.5$ eV. This has almost become a big challenge in the mid-IR NLO materials science and laser technology. For instance, the currently most used IR NLO materials, including $AgGaX_2$ (X = S, Se, Te)[16−18] or $ZnGeP_2$,[19] are inadequate for the mid-IR applications because of their low LDT or harmful two-phonons absorption principally caused by the relatively small E_g, although they have very strong NLO effects. Over the past 20 years, quite a few new chalcogenides with remarkably high IR NLO response have been discovered,[11] with the development of exploratory synthesis and theoretical simulations for the understanding of structure−property relationship. It is noteworthy that, however, the known mid-IR NLO materials are largely metal gallium/germanium/indium (Ga/Ge/In) chalcogenides. Meanwhile, a majority of these researches just focused on the SHG effect as large as possible in crystal, while the other factors that determine the mid-IR NLO performances, e.g., E_g and Δn, were not considered. Herein, under the comprehensive consideration of the conditions (I) to (IV), we highlight the family of metal thiophosphates as a very promising but long-ignored compound system for the mid-IR NLO applications. In fact, the relatively strong covalent P−S bonds can not only give rise to a relatively large NLO response, but also exhibit the high optical transmission down to the near-UV region (i.e., have wide E_g). To the best of our knowledge, the only mid-IR NLO metal thiophosphate that has been studied in detail is $InPS_4$,[20] in which the measured SHG coefficient $d_{ij} \sim 25$ pm/V and birefringence $\Delta n = 0.048$ are comparable to those of $AgGaS_2$ ($d_{36} \sim 13$ pm/V and $\Delta n = 0.053$).[16] More importantly, the bandgap of $InPS_4$ is 3.12 eV, quite larger than that of $AgGaS_2$ (~2.65 eV), strongly demonstrating the suitability of metal thiophosphates as the good mid-IR NLO materials.

In this work, the noncentrosymmetric metal thiophosphates with representatively structural features in the M−N−P−S system (M = the A-site cations, such as alkaline or alkaline earth metal cations; N = the B-site cations, such as Al^{3+}, Zn^{2+}, Cd^{2+}, In^{3+}, Sn^{2+}, Pb^{2+}, Sb^{3+}, Bi^{3+}, Ti^{4+}) are systematically investigated. The reason we focus on this type of thiophosphates is that there are no unclosed d or f electrons in the M and N cations because the d−d or f−f electronic transitions have negative influences on the enlargement of bandgap. Meanwhile, owing to the particularity (e.g., photodarkening effect[21]) of Ag^+ cations, the silver chalcogenides such as $AgGaS_2$ and $AgGeGaS_2$[22] usually exhibit smaller E_g and lower LDT than their lithium analogues such as $LiGaS_2$[23] and $Li_2Ga_2GeS_6$.[21] Thus, the noncentrosymmetric silver thiophosphate compounds including Ag_3PS_4,[24] $Ag_4P_2S_6$,[25] Ag_2KPS_4,[26] $Ag_5PS_4Cl_2$,[27] and $AgZnPS_4$[28] are not considered in our studies. On the basis of a thorough survey in the inorganic crystal structure database (ICSD, 2015−1, Version 1.9.8, by Fachinformatiionszentrum Karlsruhe, Germany), we select 23 M−N−P−S compounds with typically structural features from hundreds of metal thiophosphates. We attempt to make the microscopic structures exhibiting the diversity of structural features so that the structure−property relations can be considered as comprehensive as possible. The experimental crystallographic data for the 23 candidates are listed in Table S1 of the Supporting Information. We calculate the electronic structures, as well as linear and nonlinear optical properties of these selected crystals using the first-principles theory. Upon the analysis of the structure−property relationship, the mid-IR NLO generation capabilities of the metal thiophosphates are prospected. Several crystals are predicted to exhibit good mid-IR NLO performances with wide bandgaps and large SHG responses.

2. COMPUTATIONAL METHODS

The first-principles calculations are performed by the plane-wave pseudopotential method[29] based on density functional theory (DFT)[30] implemented in the CASTEP package.[31] The ion-electron interactions are modeled by the optimized norm-conserving pseudopotentials[32] for all constituent elements. A kinetic energy cutoff of 800 eV is chosen with Monkhorst−Pack k-point[33] meshes spanning less than 0.04 per Å^3 in the Brillouin zone. On the basis of the electronic band structure, the imaginary part of the dielectric function is calculated and the real part of the dielectric function is determined using the Kramers−Kronig transform, from which the refractive indices n (and the birefringence Δn) are obtained (at the mid-IR wavelength of 2.09 μm if not specially mentioned). Furthermore, the SHG coefficients d_{ij} are calculated using an expression originally proposed by Rashkeev et al.[34] and developed by Lin et al.[35] The corresponding powder SHG (PSHG) effect $\langle d_{powder} \rangle$ is also obtained by Kurtz−Perry method.[36] The computational details for SHG coefficients are summarized in the Supporting Information.

In order to obtain the accurate prediction of bandgap E_g, the screened exchange local density approximation (i.e., sX-LDA) method[37] is employed, which is verified to be suitable for semiconductors.[38,39] For the optical property calculations the scissors-corrected LDA method is adopted,[40,41] where the scissors operator is set as the difference between the calculated sX-LDA and LDA bandgaps. This self-consistent ab initio approach has been proven to be a very efficient and accurate way for the investigation of linear and nonlinear optical properties in many types of NLO materials without introducing any experimental parameter.[42] The calculated values of bandgaps E_g, SHG coefficients d_{ij} and birefringence Δn for the benchmark NLO materials, including KDP,[3] $ZnGeP_2$,[19] $LiGaS_2$,[23] $LiGaSe_2$,[23] $BaGa_4S_7$,[43] and $BaGa_4Se_7$,[44] are listed in Table S2 of the Supporting Information. The good agreement with the experimental results clearly demonstrates the validity of our computational methods for the present purposes. Furthermore, for analyzing the contribution of an ion (or ionic group) to the nth-order susceptibility $\chi^{(n)}$, a real-space atom-cutting technique is adopted.[35] Within this method, the contribution of ion A to the nth-order susceptibility (denoted as $\chi^{(n)}(A)$) is obtained by cutting all ions except A from the original wave functions $\chi^{(n)}(A) = \chi^{(n)}$(all ions except A are cut). Accordingly, the contributions of these active anionic units to the NLO effect and birefringence can be quantitatively determined. The relevant discussions see the Supporting Information.

3. RESULTS AND DISCUSSION

3.1. Structural and Optical Properties of Thiophosphates. In the M−N−P−S type thiophosphates, the connected patterns of the P−S anionic groups, e.g., isolated, corner-sharing $(PS_4)^{3-}$ tetrahedra and/or ethane-like $(P_2S_6)^{4-}$ units, display a great structural diversity. Further combined with the condensation of the N−S polyhedra, the zero-dimensional (0-D) discrete clusters, one-dimensional (1-D) chains, two-dimensional (2-D) layers, or three-dimensional (3-D) frameworks can be constructed. We catalogue the selected 23 metal thiophosphates to four types according to the structural features of the combined N−P−S groups: the crystals containing isolated P−S groups (see Section 3.1.1), the crystals containing the SOJT d^0/d^{10} transition metal cations, where $N = Ti^{4+}$, Cd^{2+}, etc. (see Section 3.1.2), the crystals containing the SALP cations, where $N = Sn^{2+}$, Pb^{2+}, Sb^{3+}, Bi^{3+}, etc. (see Section 3.1.3), and the crystals containing bridged N−S anionic polyhedra, where N =

DOI: 10.1021/jacs.5b07920
J. Am. Chem. Soc. 2015, 137, 13049−13059

Al^{3+}, Zn^{2+}, In^{3+}, etc. with relatively small covalent radius (see Section 3.1.4).

3.1.1. Metal Thiophosphates Containing the Isolated P−S Anionic Groups. This type of metal thiophosphates mainly include γ-Li_3PS_4,[45] α-Na_3PS_4,[46] and $K_3PS_4{\cdot}H_2O$,[47] which contain the isolated alkaline metal cations and $(PS_4)^{3-}$ anions. The electronic densities distributed on the constituent atoms (see Figure S1 in the Supporting Information) also clearly exhibit the isolated features of the basic structural units. The cations and anionic groups are accumulated by ionic interaction to crystallize in the periodical lattices. Figure 1 shows the unit

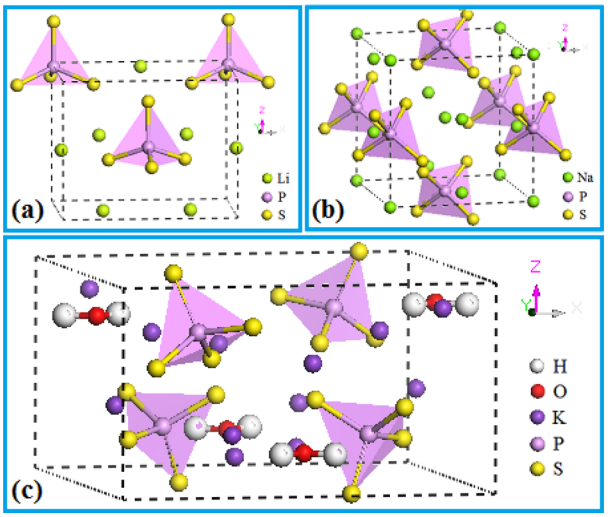

Figure 1. Structures of γ-Li_3PS_4 (a), α-Na_3PS_4 (b), and $K_3PS_4{\cdot}H_2O$ (c).

cells of these metal thiophosphates. γ-Li_3PS_4 is crystallized in the orthorhombic structure with the space group of $Pmn2_1$. The structure is composed of the close packed *A*-site Li^+ cationic spheres and the $(PS_4)^{3-}$ anionic tetrahedra which are arranged parallel to the *c*-axis but antiparallel in the *a*−*b* plane[45] (see Figure 1a). α-Na_3PS_4 is crystallized in the space group of $P\bar{4}2_1c$, and consists of *A*-stie Na^+ cations and isolated $(PS_4)^{3-}$ anions with two formula units per tetragonal unit cell. Note that all the $(PS_4)^{3-}$ tetrahedral apexes are arranged along the same direction[46] (see Figure 1b). For $K_3PS_4{\cdot}H_2O$ it is a hydrate potassium thiophosphate with the space group of $P2_12_12$, and the four $(PS_4)^{3-}$ tetrahedra are oriented differently in an orthorhombic unit cell[47] (see Figure 1c).

The calculated linear and nonlinear optical properties are listed in Table 1. It is clearly shown that all of the three compounds possess relatively wide bandgaps (E_g ~ 3.26−3.83 eV) and large SHG effects (~10−25 × KDP), thus exhibiting a very suitable balance between E_g and d_{ij} for the mid-IR NLO standard. In order to further understand the relationship between microstructures and macro-properties, the electronic structures of γ-Li_3PS_4, α-Na_3PS_4, and $K_3PS_4{\cdot}H_2O$ were calculated. The total and partial density of states (DOS/PDOS) for these crystals show that the top of valence band (VB) and the bottom of conduction band (CB) are mainly occupied by the orbitals of P and S, and the contribution from the electronic states of Li, Na and K is neglectably small (see Figure S2 in the Supporting Information). Since the optical response mainly originates from the electronic transitions between the VB and CB states close to the bandgap, the $(PS_4)^{3-}$ groups would mainly determine the optical properties of these three crystals. To confirm this point, the real-space

Table 1. Calculated E_g, d_{ij}, $\langle d_{powder}\rangle$, and Δn in γ-Li_3PS_4, α-Na_3PS_4, and $K_3PS_4{\cdot}H_2O$, Respectively[a]

	E_g (eV)	d_{ij} (pm/V)	$\langle d_{powder}\rangle$ (pm/V)	Δn
γ-Li_3PS_4	3.68	d_{15} = −3.08	3.66	0.0443
		d_{24} = −4.03		
		d_{33} = 4.32		
Li^+		d_{15} = −0.21	0.30	0.0127
		d_{24} = −0.38		
		d_{33} = 0.25		
$(PS_4)^{3-}$		d_{15} = −2.90	3.48	0.0472
		d_{24} = −3.85		
		d_{33} = 4.09		
α-Na_3PS_4	3.26	d_{14} = 9.64	8.15	0.0091
Na^+		d_{14} = 1.21	1.02	0.0018
$(PS_4)^{3-}$		d_{14} = 9.59	8.10	0.0095
$K_3PS_4{\cdot}H_2O$ 3.83		d_{14} = 3.06	2.59	0.0265
K^+		d_{14} = 0.36	0.30	0.0086
$(PS_4)^{3-}$		d_{14} = 2.73	2.31	0.0246
H_2O		d_{14} = 0.53	0.45	0.0071

[a]The atom-cutting results on the constituent cations and anionic groups are also listed.

atom-cutting method is adopted to quantitatively analyze the respective contribution of constituent cations and anionic groups in γ-Li_3PS_4, α-Na_3PS_4, and $K_3PS_4{\cdot}H_2O$ (see Table 1). It is shown that the contribution of the alkaline metal cations to both SHG effect and birefringence is less than 15% (~8%, 12% and 11% for Li^+, Na^+ and K^+, respectively), while the contribution of $(PS_4)^{3-}$ anionic groups is larger than 85% in these crystals. This conclusion is in accordance with the anionic group theory proposed by Chen for the UV and deep-UV NLO crystals.[48] Meanwhile, because the polarizations of these isolated $(PS_4)^{3-}$ units are almost aligned in one direction in α-Na_3PS_4 while not completely parallel in γ-Li_3PS_4 or $K_3PS_4{\cdot}H_2O$, the maximum SHG coefficient of the former crystal (~10 pm/V) is much larger than those of the latter crystals (~3−4 pm/V).

In addition, a binary compound P_4S_5 (with the space group $P2_1$) exhibits a pure macromolecular P−S structure,[49] in which two 0-D isolated cage-like P_4S_5 clusters have parallel polarizations along the *c*-axis in the unit cell (see Figure 2). This

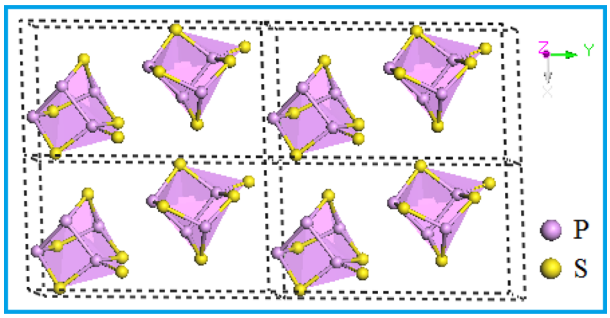

Figure 2. Periodic cluster structure of P_4S_5.

structural feature is very beneficial for the good NLO performances; the calculated results are E_g = 3.18 eV, $\langle d_{powder}\rangle$ ~ 24 × KDP with d_{16} = −4.04 pm/V, d_{14} = 5.41 pm/V, d_{22} = −1.98 pm/V, d_{23} = 9.35 pm/V, and Δn = 0.054. In particular, the much larger birefringence in P_4S_5, compared with the classical binary NLO crystals (e.g., GaAs, Δn ~ 0), makes its phase-matchability more suitable for mid-IR harmonic generation. The shortest SHG wavelength in this crystal achieve at

DOI: 10.1021/jacs.5b07920
J. Am. Chem. Soc. 2015, 137, 13049−13059

about 900 nm (see Figure S3 in the Supporting Information). Thus, we predict that P_4S_5 can produce the direct SHG output of the 2.09 μm lasers which are widely used currently. Considering that usually a binary compound system is relatively easy to be synthesized and grown, P_4S_5 might be a very promising material for the practical mid-IR NLO applications.

The above first-principles studies reveal that (1) the strong P−S bonds can enlarge the bandgap to the level of wide-gap semiconductor (E_g > 3.0 eV), and (2) the parallel arrangement of isolated $(PS_4)^{3-}$ or P_4S_5 polar groups can improve the SHG effect to the level of $AgGaS_2$ ($d_{ij} \sim 10-25 \times$ KDP). For instance, γ-Li_3PS_4 possesses almost the same E_g (3.68 eV vs 3.87 eV) and Δn (0.044 vs 0.040) as the IR NLO crystal $LiGaS_2$.[23] At the same time, the SHG effect in γ-Li_3PS_4 satisfies the elementary requirement for good mid-IR NLO crystal (>10 × KDP). This clearly demonstrates the potential of metal thiophosphate system as the promising mid-IR NLO crystals is comparable to that of classical metal gallium chalcogenides. However, note that the isolated $(PS_4)^{3-}$ tetrahedra usually have the relatively low optical anisotropy, thus this anionic group itself is some difficult to achieve the preferred balance between d_{ij} and E_g (i.e., d_{ij} > 20× KDP and E_g > 3.5 eV), and the birefringence values in this type of thiophosphates are relatively small (typically Δn < 0.04). In order to improve the mid-IR NLO performances, it would be a good strategy by introducing the *B*-site cations to interact with the S^{2-} anions.

3.1.2. Metal Thiophosphates Containing the SOJT Cations. The SOJT effect is most often encountered in the metal oxides, but this effect can occur in sulfides as well.[50−53] The SOJT effect could also occur in the other ionic coordination environments apart from the octahedral shape.[54−57] However, herein we only consider the metal thiophosphates with the SOJT octahedra containing the d^0/d^{10} transition metal cations (e.g., $(TiS_6)^{8-}$ and $(CdS_6)^{10-}$ groups), despite the scarce number of these compounds in the known thiophosphates.

The selected compounds in this type of compounds include TiP_2S_6[58] and $Cd_2P_2S_6$.[59] Their structures are displayed in Figure 3. In TiP_2S_6 every two P atoms make a pair, while tetrahedrally

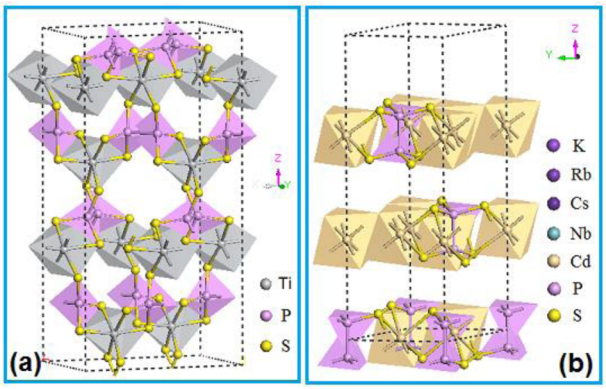

Figure 3. Structures of TiP_2S_6 (a) and $Cd_2P_2S_6$ (b).

surrounding by three S atoms for each P atom, forming a $(P_2S_6)^{4-}$ group.[58] The P−P atom pairs are all parallel to the *c*-axis, so that the $(P_2S_6)^{4-}$ groups are linked one another by the Ti−S bonds approximately in the direction of the P−P axes with the *Fdd*2 space group (see Figure 3a). In this way the Ti^{4+} cations have a distorted octahedral coordination with S^{2-} anions, and the Ti−S distances are ranged from 2.433 to 2.454 Å. As a comparison, the cadmium thiophosphate $Cd_2P_2S_6$[59] crystallizes in the trigonal symmetry with *R*3 space group. Each ethane-like $(P_2S_6)^{4-}$ group is linked by six edge-sharing $(CdS_6)^{10-}$ octahedral groups with the Cd−S lengths ranging from 2.706 to 2.750 Å (see Figure 3b). In both compounds the $(P_2S_6)^{4-}$ units are connected with the $(TiS_6)^{8-}$ or $(CdS_6)^{10-}$ groups to form the 3-D or 2-D multiple *N*−P−S (*N* = Ti, Cd) frameworks.

Table 2 lists the calculated E_g, d_{ij}, $\langle d_{powder}\rangle$, and Δn for TiP_2S_6 and $Cd_2P_2S_6$. In $Cd_2P_2S_6$ the NLO response is rather small (~2 × KDP) because of the approximately centrosymmetric arrangement of the basic building units. As a comparison, TiP_2S_6 possesses much stronger SHG effect (~30 × KDP) due to the almost parallel arrangement of the microscopic groups. Moreover, both compounds exhibit a large birefringence (Δn > 0.25). These results demonstrate that the enhanced optical anisotropy (i.e., large SHG response and birefringence) can be obtained by introducing the SOJT cations in the metal thiophosphates, if the arrangement of optical active microscopic groups is parallel. Nevertheless, the bandgaps in these thiophosphates are relatively small (E_g < 3.0 eV) because in the electronic band structures the Ti or Cd orbitals are mainly occupied at the CB minimum (CBM) which narrow the bandgaps (see Figure S2 in the Supporting Information).

Table 2. Calculated E_g, d_{ij}, $\langle d_{powder}\rangle$, Δn and Atom-Cutting Results in TiP_2S_6 and $Cd_2P_2S_6$

	E_g (eV)	d_{ij} (pm/V)	$\langle d_{powder}\rangle$ (pm/V)	Δn
TiP_2S_6	2.57	d_{15} = 15.45	10.82	0.3321
		d_{24} = 3.28		
$(P_2S_6)^{4-}$		d_{15} = 8.51	5.95	0.2817
		d_{24} = 1.76		
$Cd_2P_2S_6$	2.82	$d_{11} = -d_{12} = -0.95$	0.66	0.2778
$(P_2S_6)^{4-}$		$d_{11} = -d_{12} = -0.83$	0.57	0.2611

The further atom-cutting analysis (in Table 2) reveals that the optical anisotropy in these metal thiophosphates is both contributed by the $(P_2S_6)^{4-}$ and $(TiS_6)^{8-}/(CdS_6)^{10-}$ anionic groups, although the contribution from $(P_2S_6)^{4-}$ groups is dominant (more than 55% and 85% to the overall birefringence and SHG effect, respectively). Moreover, the Mulliken populations analysis[60] (see Table S3 in the Supporting Information) shows that the bond populations on Ti−S/Cd-S (~0.25−0.42) are smaller than those on P−S (~0.53−0.62), indicating that the covalent characteristic of Ti−S/Cd−S bonds is weaker than that of P−S bonds.

In summary, the birefringence and SHG effect of the metal thiophosphates containing the SOJT cations can be significantly improved compared to the structures with isolated $(PS_4)^{3-}$ groups. Nevertheless, the relatively small E_g (<3.0 eV) means that the required balance between d_{ij} and E_g could not be achieved well in these crystals. Actually, the narrowing of energy bandgap in this type of thiophosphates is rational. It is because intrinsically the SOJT effect is resulted from the interaction between the highest occupied molecular orbitals (HOMO) and the lowest unoccupied molecular orbitals (LUMO).[54−57] This implies that the energy bandgaps for the thiophosphate system containing the SOJT cations could not be large. Otherwise, the interaction between HOMO and LUMO would be very small and the SOJT effect would vanish. Therefore, one may conclude that in general it is some difficult to find a candidate possessing the desirably comprehensive capabilities for mid-IR NLO performances in this type of metal thiophosphates.

DOI: 10.1021/jacs.5b07920
J. Am. Chem. Soc. 2015, 137, 13049−13059

3.1.3. Metal Thiophosphates Containing the SALP Cations. These metal thiophosphates include $Pb_3P_2S_8$,[61] α-$Na_6Pb_3P_4S_{16}$,[62] $RbPbPS_4$,[63] $K_9BiP_4S_{16}$,[64] with $(PS_4)^{3-}$ units, and β-$NaSbP_2S_6$,[65] $KSbP_2S_6$,[66] $KBiP_2S_6$,[67] with $(P_2S_6)^{4-}$ units. Their structures are displayed in Figure 4. The cubic $Pb_3P_2S_8$

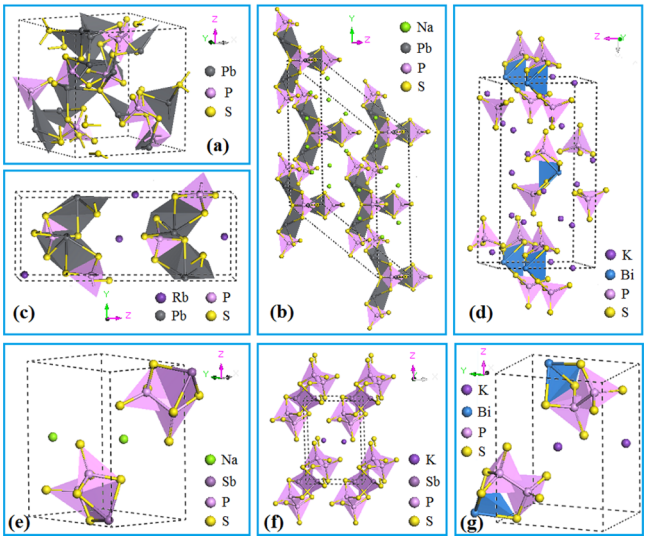

Figure 4. Structures of $Pb_3P_2S_8$ (a), α-$Na_6Pb_3P_4S_{16}$ (b) $RbPbPS_4$ (c), $K_9BiP_4S_{16}$ (d), β-$NaSbP_2S_6$ (e), $KSbP_2S_6$ (f), and $KBiP_2S_6$ (g).

with $P2_13$ space group consists of $(PS_4)^{3-}$ tetrahedra connected with irregular $(PbS_8)^{14-}$ polyhedra[61] (see Figure 4a). The crystal of α-$Na_6Pb_3(PS_4)_4$ contains the saucer-shaped $(Pb_3(PS_4)_4)^{6-}$ molecular cluster with the C_{3v} symmetry, which enables itself columnar stacking along the *c*-axis[62] (see Figure 4b). $RbPbPS_4$ crystallizes in space group $P2_12_12_1$ of the orthorhombic system. The structure consists of 2-D $(PbPS_4)^-$ layers built from $(PbS_7)^{12-}$ monocapped trigonal prisms and $(PS_4)^{3-}$ tetrahedra, which are separated by Rb^+ ions[63] (see Figure 4c). Bright-red $K_9BiP_4S_{16}$ crystallizes in the orthorhombic space group $P2_12_12$ and have a discrete molecular salt structure with mononuclear $(Bi(PS_4)_4)^{9-}$ complexes[64] (see Figure 4d). β-$NaSbP_2S_6$, $KSbP_2S_6$, and $KBiP_2S_6$ are all crystallized in the monoclinic space group $P2_1$. They are formed by the combined anionic groups of ethane-like $(P_2S_6)^{4-}$ units and $(NS_3)^{3-}$ pyramids (N = Sb, Bi) separated by Na^+ or K^+cations[65−67] (see Figure 4e, 4f and 4g). Among these compounds the bandgap of β-$NaSbP_2S_6$ only has been determined by UV−vis diffuse reflectance experiments.[65] The measured value of 2.25 eV is consistent with our first-principles result (2.66 eV).

In these compounds, the SALP cations N are coordinated with S^{2-} anions, forming $(PbS_4)^{6-}$ groups in $Pb_3P_2S_8$ (Figure 4a) and α-$Na_6Pb_3P_4S_{16}$ (Figure 4b), $(PbS_5)^{8-}$ groups in $RbPbPS_4$ (Figure 4c), $(SbS_3)^{3-}$ groups in β-$NaSbP_2S_6$ (Figure 4e) and $KSbP_2S_6$ (Figure 4f), and $(BiS_3)^{3-}$ groups in $K_9BiP_4S_{16}$ (Figure 4d) and $KBiP_2S_6$ (Figure 4g). The produced 0-D, 1-D or 2-D N−P−S anionic frameworks significantly strengthen the structural anisotropy. Table 3 lists the calculated E_g, d_{ij}, $\langle d_{powder}\rangle$ and Δn for these seven compounds. Clearly, the SHG effect and birefringence are greatly enhanced compared to the compounds with isolated $(PS_4)^{3-}$ groups. The further atom-cutting analysis (also see Table 3) reveals that the N−P−S anionic groups have the major contribution to the NLO effect and birefringence (>85% for $\langle d_{powder}\rangle$ and Δn) in these structures. The $(PS_4)^{3-}$ or $(P_2S_6)^{4-}$ groups contribute more than half of optical anisotropy

Table 3. Calculated E_g, d_{ij}, $\langle d_{powder}\rangle$, Δn and Atom-Cutting Results in $Pb_3P_2S_8$, α-$Na_6Pb_3P_4S_{16}$, $RbPbPS_4$, $K_9BiP_4S_{16}$, β-$NaSbP_2S_6$, $KSbP_2S_6$, and $KBiP_2S_6$, Respectively

	E_g (eV)	d_{ij} (pm/V)	$\langle d_{powder}\rangle$ (pm/V)	Δn
$Pb_3P_2S_8$	2.61	d_{14} = 6.33	5.35	0.0000
$(PS_4)^{3-}$		d_{14} = 5.03	4.25	0.0000
α-$Na_6Pb_3P_4S_{16}$	2.80	$d_{11} = -d_{12}$ = 17.86	13.03	0.0814
		$d_{15} = d_{24}$ = −3.34		
		d_{33} = 8.40		
$(PS_4)^{3-}$		$d_{11} = -d_{12}$ = 16.10	11.94	0.0889
		$d_{15} = d_{24}$ = −4.32		
		d_{33} = 4.48		
$(Pb_3P_4S_{16})^{6-}$		$d_{11} = -d_{12}$ = 18.09	13.14	0.1194
		$d_{15} = d_{24}$ = −3.46		
		d_{33} = 7.52		
$RbPbPS_4$	3.01	d_{14} = 0.23	0.19	0.1757
$(PS_4)^{3-}$		d_{14} = 0.30	0.25	0.1207
$(PbPS_4)^-$		d_{14} = 0.26	0.21	0.1915
$K_9BiP_4S_{16}$	2.49	d_{14} = 5.22	4.41	0.1053
$(PS_4)^{3-}$		d_{14} = 3.03	2.56	0.0978
$(BiP_4S_{16})^{9-}$		d_{14} = 5.02	4.24	0.1129
β-$NaSbP_2S_6$	2.66	d_{14} = 3.13	16.99	0.0622
		d_{22} = −37.47		
		d_{23} = −4.27		
$(P_2S_6)^{4-}$		d_{14} = 2.29	9.64	0.0650
		d_{22} = −21.69		
		d_{23} = −1.28		
$(SbP_2S_6)^-$		d_{14} = 3.18	17.11	0.0616
		d_{22} = −37.77		
		d_{23} = −4.25		
$KSbP_2S_6$	2.98	d_{14} = 3.66	10.48	0.1618
		d_{22} = −21.39		
		d_{23} = −4.04		
$(P_2S_6)^{4-}$		d_{14} = 3.68	6.90	0.1337
		d_{22} = −13.58		
		d_{23} = −1.87		
$(SbP_2S_6)^-$		d_{14} = 3.70	10.42	0.1602
		d_{22} = −21.25		
		d_{23} = −4.00		
$KBiP_2S_6$	2.80	d_{16} = −5.60	7.97	0.0342
		d_{22} = 18.70		
$(P_2S_6)^{4-}$		d_{16} = −3.00	5.54	0.0429
		d_{22} = 13.27		
$(BiP_2S_6)^-$		d_{16} = −5.71	7.88	0.0323
		d_{22} = 18.44		

in the total N−P−S groups (>55% for $\langle d_{powder}\rangle$ and Δn generally), whereas the lone-pair Pb^{2+}, Sb^{3+}, and Bi^{3+} cations in the polar N−S groups make the significant contribution as well. Thus, most of these compounds exhibit relatively strong d_{ij} (>10 × KDP), and their birefringence values are much larger ($\Delta n \approx$ 0.08−0.18 for α-$Na_6Pb_3P_4S_{16}$, $RbPbPS_4$, $K_9BiP_4S_{16}$, $KSbP_2S_6$, and 0.03−0.06 for β-$NaSbP_2S_6$, $KBiP_2S_6$) than those of γ-Li_3PS_4, α-Na_3PS_4, and $K_3PS_4{\cdot}H_2O$ ($\Delta n \approx$ 0.01−0.04).

Because of the nonparallel arrangements of $(PbS_4)^{6-}$ and $(PS_4)^{3-}$ groups in $Pb_3P_2S_8$ (see Figure 4a) and head-to-head arrangements of the polar $(BiS_3)^{3-}$ units in $K_9BiP_4S_{16}$ (see Figure 4d), the two compounds exhibit much smaller SHG responses (~14 × KDP) than that in $Na_6Pb_3P_4S_{16}$ in which the nearly parallel arrangements and additive polarizations of Pb−S and P−S units (see Figure 4b) give rise to the SHG effect about 50 × KDP. In $RbPbPS_4$ the nearly centric structure (see Figure

DOI: 10.1021/jacs.5b07920
J. Am. Chem. Soc. 2015, 137, 13049−13059

4c) makes its SHG effect close to only one-half of KDP. Although a single $(P_2S_6)^{4-}$ group in β-$NaSbP_2S_6$, $KSbP_2S_6$, and $KBiP_2S_6$ seems to be "head-to-head" (see Figure 4e, 4f and 4g), the asymmetric coordination environments around the cations *N* make the $(P_2S_6)^{4-}$ groups produce some distortions (e.g., the six bond lengths of the $(P_2S_6)^{4-}$ groups in $NaSbP_2S_6$ are varied from 1.9693 to 2.0580 Å), thus the contribution of P−S units to total polarization is very large (>50%). It is the synergetic effect of distorted $(P_2S_6)^{4-}$ and polar *N*−S groups that results in a relatively strong SHG response in β-$NaSbP_2S_6$, $KSbP_2S_6$, and $KBiP_2S_6$ (~96, 55, and 48 × KDP, respectively).

However, the PDOS analysis (see Figure S2 in the Supporting Information) reveals that the electronic orbitals on the SALP cations *N* (*N* = Pb, Sb, Bi) occupy at the CBM and determine the bandgaps in these metal thiophosphates. As a result, most of these compounds display the bandgaps (~2.50−3.00 eV) comparable to that of $AgGaS_2$ (~2.68 eV), though larger than that of $ZnGeP_2$ (~2.00 eV). Overall, the metal thiophosphates containing the SALP cations exhibit relatively large NLO effects but rather small bandgaps. Among these compounds only the $KSbP_2S_6$ crystal satisfies the elementary requirement for the good mid-IR NLO performance with the balance between d_{ij} (~55 × KDP) and E_g (~3.00 eV).

In addition, there are two metal thiophosphates $TlSnPS_4$[68] and $TlBiP_2S_6$[69] which contain two different types of SALP cations. $TlSnPS_4$ crystallizes in the space group of $Pna2_1$ to exhibit the edge-sharing $(SnPS_4)^-$ network[68] (see Figure 5a),

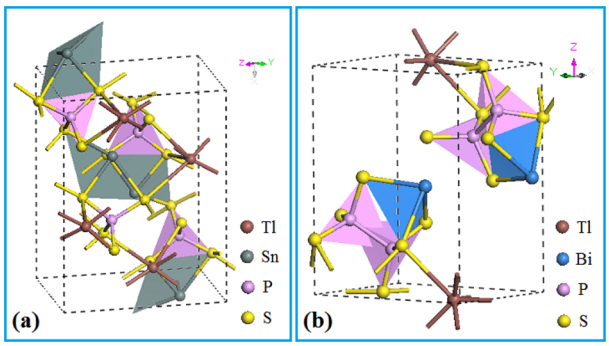

Figure 5. Structures of $TlSnPS_4$ (a) and $TlBiP_2S_6$ (b).

while $TlBiP_2S_6$ are isostructural with $KBiP_2S_6$[69] (see Figure 5b). In these crystals, Tl^+ is another SALP cation besides the Sn^{2+} or Bi^{3+} SALP cation, and possesses some covalent interactions with the coordinated S^{2-} anions. The linear and nonlinear optical properties in these compounds are shown in Table 4. It is found that these compounds exhibit much larger d_{ij} but rather smaller E_g compared with those containing one type of *N* cations only. This indicates that the introduction of additional SALP Tl^+ cations has positive influence on the improvement of NLO response but negatively affects the enlargement of bandgap for this type of structures.

3.1.4. Metal Thiophosphates Containing Bridged N−S Polyhedra Where N Has Small Covalent Radius. It has been shown that in metal thiophosphates the introduction of SOJT or SALP *N* cations can significantly enlarge the SHG response and birefringence, but inevitably narrows the bandgap (typically <3.0 eV) compared with the isolated P−S groups due to the presence of the CBM electronic states on the *N* cations. In order to increase the bandgap while maintaining the large SHG effect and birefringence, we consider to adopt the metal cations *N* with

Table 4. Calculated E_g, d_{ij}, $\langle d_{powder}\rangle$, Δn and Corresponding Atom-Cutting Results in $TlSnPS_4$ and $TlBiP_2S_6$, Respectively

	E_g (eV)	d_{ij} (pm/V)	$\langle d_{powder}\rangle$ (pm/V)	Δn
$TlSnPS_4$	1.65	d_{15} = −9.30	6.20	0.1229
		d_{24} = 2.75		
		d_{33} = 8.14		
$(PS_4)^{3-}$		d_{15} = −5.75	4.35	0.1101
		d_{24} = 3.93		
		d_{33} = 5.47		
$TlBiP_2S_6$	2.22	d_{16} = −7.30	14.28	0.1551
		d_{22} = 32.73		
		d_{23} = −9.65		
$(P_2S_6)^{4-}$		d_{16} = −2.69	9.89	0.1291
		d_{22} = 23.94		
		d_{23} = −5.02		

relatively small covalent radius, such as *N* = Zn^{2+}, Al^{3+} or In^{3+}. By introducing these cations into the thiophosphates, the parallel polarized *N*−S tetrahedra/octahedra combine with P−S units to construct the anisotropic covalent *N*−P−S frameworks in crystal, as in the examples of $Zn_3(PS_4)_2$,[70] $LiZnPS_4$,[70] $InPS_4$,[71] $KInP_2S_7$,[72] lt-$AlPS_4$,[73] ht-$AlPS_4$,[73] $Al_4(P_2S_6)_3$,[73] and $NaAlP_2S_6$.[74] Their structures are displayed in Figure 6.

The $Zn_3(PS_4)_2$ compound crystallizes in space group $P\bar{4}n2$. The $(PS_4)^{3-}$ tetrahedra are arranged according to the motif of the cubic closest packing, and the Zn^{2+} cations are located in three-quarters of the tetrahedral voids, forming the corner-sharing $(ZnS_4)^{4-}$ tetrahedra[70] (see Figure 6a). The structure of $LiZnPS_4$ is analogous to that of $Zn_3(PS_4)_2$, but one of the two Zn cations is replaced by two Li cations in each chemical formula. In the packing of the $(PS_4)^{3-}$ units all the tetrahedral voids are occupied by lithium or zinc cations, with the space group of $I\bar{4}$[70] (see Figure 6b). The similar 3-D framework structure is also presented in $InPS_4$, in which the $LiZnPS_4$ structure is modified by removing all Li^+ cations and substituting In^{3+} cations for Zn^{2+} cations in the tetrahedral voids[71] (see Figure 6c). $KInP_2S_7$ crystallizes in the monoclinic space group C2, with a 3-D framework that built from the bitetrahedral $(P_2S_7)^{4-}$ units sharing edges and corners with $(InS_6)^{9-}$ octahedra[72] (see Figure 6d). For the aluminum thiophosphates, they exhibit various structural features, such as 1-D $(AlS_4-PS_4)_\infty$ chains in the fibrous needle-like lt-$AlPS_4$ and the platelet-like ht-$AlPS_4$ phases[73] (see Figure 6e and 6f), 2-D $(Al-P_2S_4-Al)_\infty$ layers in the monoclinic $Al_4(P_2S_6)_3$[73] (see Figure 6g), and 3-D networks in the orthorhombic $NaAlP_2S_6$[74] (see Figure 6h).

The calculated E_g, d_{ij}, $\langle d_{powder}\rangle$ and Δn for these compounds are listed in Table 5. Clearly, these 1-D, 2-D and 3-D thiophosphate structures, such as corner-sharing ZnS_4-PS_4 (Figure 6a and 6b), InS_4-PS_4 (Figure 6c) and edge-sharing $InS_6-P_2S_7$ (Figure 6d), AlS_4-PS_4 (Figure 6e and 6f), $AlS_6-P_2S_6$ (Figure 6g and 6h) anionic groups, can enlarge the bandgaps to more than 3.0 eV. Meanwhile, the enhanced structural anisotropy can result in the strong NLO effect (d_{ij} > 10 × KDP) and large birefringence (Δn > 0.04).

In details, the bandgaps of $Zn_3(PS_4)_2$ (3.19 eV), $LiZnPS_4$ (3.76 eV), $InPS_4$ (3.44 eV), $KInP_2S_7$ (3.53 eV), lt-$AlPS_4$ (3.47 eV), ht-$AlPS_4$ (3.61 eV), $Al_4(P_2S_6)_3$ (2.91 eV) and $NaAlP_2S_6$ (3.53 eV) are comparable to those of Li_3PS_4 (3.68 eV), Na_3PS_4 (3.26 eV) and $K_3PS_4{\cdot}H_2O$ (3.83 eV), and larger than the values of the compounds (~2.5 eV) discussed in the 3.1.2 and 3.1.3 sections. The Mulliken analysis[60] (see Table S3 in the Supporting Information) reveals that the Zn−S (In−S, or Al−

DOI: 10.1021/jacs.5b07920
J. Am. Chem. Soc. 2015, 137, 13049−13059

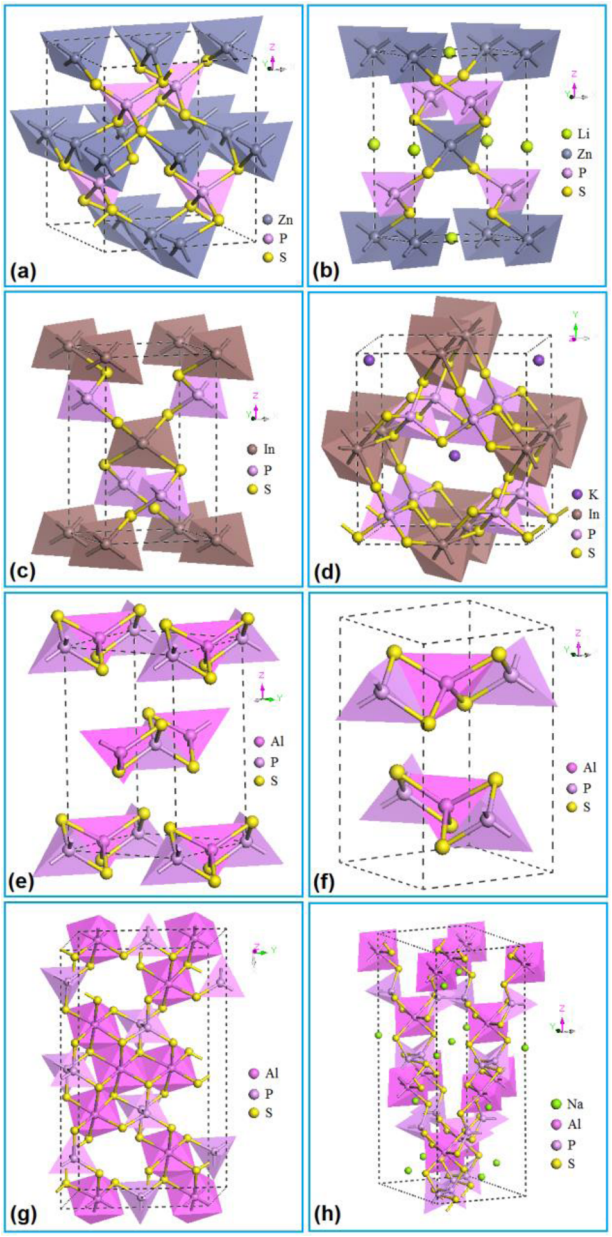

Figure 6. Structures of $Zn_3(PS_4)_2$ (a), $LiZnPS_4$ (b), $InPS_4$ (c), $KInP_2S_7$ (d), lt-$AlPS_4$ (e), ht-$AlPS_4$ (f), $Al_4(P_2S_6)_3$ (g) and $NaAlP_2S_6$ (h).

S) bonds have larger bond populations (or higher covalency) and smaller bond lengths than the Ti−S (Cd−S, Sn−S, Pb−S, Sb−S, or Bi−S) bonds. Moreover, the PDOS plots (see Figure S2 in the Supporting Information) show the stronger hybridization of electronic electrons at the top of VB on the former bonds compared with the latter bonds. This means that the nonbonding orbitals on the sulfur atoms are effectively saturated by the electrons on the coordinated *N* cations with relatively small covalent radius, analogous to the case of $RbAlCO_3F_2$.[75] Thus, the thiophosphates containing covalent Al^{3+}, Zn^{2+} or In^{3+} cations (e.g., $NaAlP_2S_6$, $LiZnPS_4$, and $InPS_4$) exhibit larger bandgaps than those containing the SOJT or SALP *N* cations (e.g., TiP_2S_6, $Na_6Pb_3P_4S_{16}$, $NaSbP_2S_6$, and $KBiP_2S_6$). More importantly, the enlargement of the bandgaps does not result in the decrease of SHG effects in these compounds (~42 × KDP for $Zn_3(PS_4)_2$, 27 × KDP for $LiZnPS_4$, 39 × KDP for $InPS_4$, 18 × KDP for $KInP_2S_7$, 11 × KDP for lt-$AlPS_4$, 16 × KDP for ht-$AlPS_4$, 14 × KDP for $Al_4(P_2S_6)_3$, and 10 × KDP for $NaAlP_2S_6$), owing to the presence of anisotropic covalent groups with parallel polarized arrangements. In addition, these compounds display various birefringence values ranged from 0.024 to 0.473.

Therefore, in this type of compounds almost all members satisfy the elementary requirement for mid-IR harmonic generation (E_g > 3.0 eV and d_{ij} > 10 × KDP). In particular, for $LiZnPS_4$ the diamond-like structure combined with the strong ionic Li^+ cations enlarges the bandgap E_g as large as that of $LiGaS_2$, and the presence of Zn^{2+} cations prompts the formation of polar framework analogous to the structure of

Table 5. Calculated E_g, d_{ij}, $\langle d_{powder}\rangle$, Δn and Corresponding Atom-Cutting Results in $Zn_3(PS_4)_2$, $LiZnPS_4$, $InPS_4$, $KInP_2S_7$, lt-$AlPS_4$, ht-$AlPS_4$, $Al_4(P_2S_6)_3$ and $NaAlP_2S_6$, Respectively

	E_g (eV)	d_{ij} (pm/V)	$\langle d_{powder}\rangle$ (pm/V)	Δn
$Zn_3(PS_4)_2$	3.19	$d_{15} = -d_{24} = 16.28$	12.51	0.0358
$(PS_4)^{3-}$		$d_{15} = -d_{24} = 12.03$	9.24	0.0291
$LiZnPS_4$	3.76	$d_{15} = -d_{24} = 0.89$	8.83	0.0725
		$d_{14} = 10.42$		
$(PS_4)^{3-}$		$d_{15} = -d_{24} = 0.94$	6.98	0.0668
		$d_{14} = 8.21$		
$(ZnPS_4)^-$		$d_{15} = -d_{24} = 0.89$	8.71	0.0691
		$d_{14} = 10.27$		
$InPS_4$	3.44	$d_{15} = -d_{24} = 13.98$	16.69	0.0234
		$d_{14} = 15.12$		
$(PS_4)^{3-}$		$d_{15} = -d_{24} = 11.51$	13.50	0.0237
		$d_{14} = 12.07$		
$KInP_2S_7$	3.35	$d_{16} = -6.85$	5.60	0.0778
		$d_{14} = -4.34$		
		$d_{22} = 1.02$		
		$d_{23} = 2.84$		
$(P_2S_7)^{4-}$		$d_{16} = -6.47$	4.93	0.0678
		$d_{14} = -3.29$		
		$d_{22} = 2.63$		
		$d_{23} = 2.94$		
$(InP_2S_7)^-$		$d_{16} = -6.59$	5.41	0.0738
		$d_{14} = -4.20$		
		$d_{22} = 1.14$		
		$d_{23} = 2.90$		
lt-$AlPS_4$	3.47	$d_{14} = 4.33$	3.66	0.2172
$(PS_4)^{3-}$		$d_{14} = 4.70$	3.97	0.1631
ht-$AlPS_4$	3.61	$d_{14} = 6.14$	5.19	0.0601
$(PS_4)^{3-}$		$d_{14} = 6.52$	5.51	0.0330
$Al_4(P_2S_6)_3$	2.91	$d_{16} = 3.29$	2.99	0.4734
		$d_{14} = -1.14$		
		$d_{22} = -5.56$		
		$d_{23} = 0.47$		
$(P_2S_6)^{4-}$		$d_{16} = 3.61$	2.97	0.4551
		$d_{14} = -0.92$		
		$d_{22} = -5.16$		
		$d_{23} = 0.50$		
$NaAlP_2S_6$	3.53	$d_{16} = -2.72$	2.50	0.2247
		$d_{24} = -1.46$		
		$d_{33} = 4.08$		
$(P_2S_6)^{4-}$		$d_{16} = -2.43$	2.55	0.2232
		$d_{24} = -1.65$		
		$d_{33} = 4.60$		
$(AlP_2S_6)^-$		$d_{16} = -2.57$	2.40	0.2288
		$d_{24} = -1.44$		
		$d_{33} = 3.96$		

DOI: 10.1021/jacs.5b07920
J. Am. Chem. Soc. 2015, 137, 13049−13059

$ZnGeP_2$. We predict that this compound can achieve the excellent balance of E_g and d_{ij} between $LiGaS_2$ and $ZnGeP_2$; its large bandgap (E_g = 3.76 eV) and the strong SHG effect (d_{ij} = 27 × KDP) satisfy the preferred requirements (E_g > 3.5 eV and d_{ij} > 20 × KDP) for the good mid-IR NLO performances. Moreover, the moderate birefringence (Δn = 0.073) is very suitable to achieve the mid-IR phase-matching condition for the practical applications.

3.2. Prospect for Metal Thiophosphates As Mid-IR NLO Crystals. In order to evaluate the prospect of thiophosphates for the mid-IR NLO applications, we summarize their NLO performances, mainly E_g and d_{ij}, and compare with other representative mid-IR NLO crystals. These compared materials include most of known mid-IR NLO crystal types and are catalogued as follows according to different kinds of elemental compositions: (1) typical IR NLO sulfides, such as $AgGaS_2$,[16] Ag_3AsS_3,[76] $HgGa_2S_4$,[77] $AgGeGaS_4$,[22] $LiGaS_2$,[23] $LiInS_2$,[78] $Li_2Ga_2GeS_6$,[21] $Li_2In_2SiS_6$,[79] $Li_2In_2GeS_6$,[79] Li_2CdGeS_4,[80] Li_2CdSnS_4,[80] Li_2MnGeS_4,[81] $BaGa_4S_7$,[43] $BaGa_2SiS_6$,[82] $BaGa_2GeS_6$,[82] $SnGa_4S_7$,[83] $SnGa_2GeS_6$,[84] $PbGa_4S_7$,[85] $NaBa_4Ge_3S_{10}Cl$,[86] $LiAsS_2$,[87] Sm_4GaSbS_9,[88] La_4InSbS_9,[89] Ba_2BiInS_5,[90] $K_2Ta_2AsS_{11}$,[50] $K_2Hg_3Ge_2S_8$,[91] $Ba_4CuGa_5S_{12}$,[92] $Rb_4Ta_2S_{11}$,[93] $Ba_8Sn_4S_{15}$,[94] and $Ba_{23}Ga_8Sb_2S_{38}$;[95] (2) typical IR NLO diselenides and tellurides, such as $AgGaSe_2$,[17] $AgGaTe_2$,[18] $Ag_3Ga_3SiSe_8$,[96] $ZnGeP_2$,[19] GaSe,[97] $LiGaSe_2$,[23] $LiGaTe_2$,[23] $LiInSe_2$,[78] $LiGaGe_2Se_6$,[98] $Li_2In_2SiSe_6$,[79] $Li_2In_2GeSe_6$,[79] $Li_2ZnGeSe_4$,[99] $Li_2ZnSnSe_4$,[99] $BaGa_4Se_7$,[44] $BaAl_4Se_7$,[100] $BaGa_2SiSe_6$,[82] $BaGa_2GeSe_6$,[82] $SnGa_4Se_7$,[83] $PbGa_2SiSe_6$,[101] $PbGa_2GeSe_6$,[101] $CsBa_3Ga_5Se_{10}Cl_2$,[102] $K_2P_2Se_6$,[103] $CsZrPSe_6$,[104] $NaAsSe_2$,[38] $KPSe_6$,[105] $RbPSe_6$,[105] $CsPSe_6$,[106] $Na_2Ge_2Se_5$,[107] $K_4GeP_4Se_{12}$,[108] $RbNb_2PSe_{10}$,[109] $Cs_5BiP_4Se_{12}$,[110] and $Pb_4Ga_4GeSe_{12}$;[111] (3) typical IR NLO halides, such as $CsGeCl_3$,[112] $CsGeBr_3$,[113] $CsGeI_3$,[114,115] $CsCdBr_3$,[116] $CsHgBr_3$,[117] $Cs_2Hg_3I_8$,[118] $NaSb_3F_{10}$,[119] SbF_3,[120] $HgBr_2$,[121] Tl_3PbBr_5,[122] KIO_2F_2,[123] Hg_2BrI_3,[124] Hg_2Br_3I,[125] $Cs_2HgCl_2I_2$,[126] and $Rb_2CdBr_2I_2$;[15] and (4) typical IR NLO oxides, such as Pb_3SeO_5,[14] $BaNbO(IO_3)_5$,[127] $BiO(IO_3)$,[128] $Li_2Ti(IO_3)_6$,[129] $Ag_2Te_3Mo_3O_{16}$,[130] $Na_2Te_3Mo_3O_{16}$,[131] $Cs_2TeMo_3O_{12}$,[132] $BaTeMo_2O_9$,[13] $RbMoIO_6$,[133] $ZnTeMoO_6$,[134] $InNb(TeO_4)_2$,[135] $Se_2B_2O_7$,[136] $Pb_2B_5O_9I$,[137] Cd_4BiBO_{10},[138] $LiIO_3$,[139] $Pb_{17}O_8Cl_{18}$,[140] $Bi_2Te(IO_3)O_5Cl$,[141] LN,[7] and KTP.[4] Their experimental NLO capabilities (d_{ij} and E_g) are listed in Table S4 of the Supporting Information. The distribution of E_g with respect to d_{ij} for all these compounds is displayed in Figure 7, from which some characteristics can be deduced: (1) A majority of the IR NLO sulfides, diselenides and tellurides (especially the latter two) possess very strong SHG effects (the largest value is about 733 × KDP for $NaAsSe_2$[38]) but relatively narrow bandgaps (typically <3.0 eV). They are mainly located in the upper left area. (2) A majority of the IR NLO halides have wide bandgaps (the largest value is about 5.0 eV for $NaSb_3F_{10}$[119]) but relatively small SHG effects (typically <10 × KDP). They are mainly located in the bottom right area. (3) There are totally 13 sulfides (i.e., $LiGaS_2$,[23] $LiInS_2$,[78] $Li_2Ga_2GeS_6$,[21] $Li_2In_2SiS_6$,[79] $Li_2In_2GeS_6$,[79] Li_2CdGeS_4,[80] Li_2MnGeS_4,[81] $BaGa_4S_7$,[43] $BaGa_2SiS_6$,[82] $BaGa_2GeS_6$,[82] $SnGa_4S_7$,[83] $PbGa_4S_7$,[85] and $NaBa_4Ge_3S_{10}Cl$[86]) and two diselenides (i.e., $LiGaSe_2$,[23] and $BaAl_4Se_7$[100]) that exhibit suitable balance between d_{ij} and E_g, locating in the blue/green area. These compounds are mostly deduced from the $AgGaS_2$/$AgGaSe_2$ parent structure by replacing the Ag^+ cations with the alkaline/alkaline-earth cations. For the halides only one compound HgBr lies in the blue area. (4) Although there are seven IR oxides located in the blue/green area, their relatively strong IR optical absorption might limit the transparency for the mid-IR generation, and then deteriorate the NLO performances in this spectral region. In addition, the very recent researches on the systems combined halides with oxides (e.g., $Pb_{17}O_8Cl_{18}$,[140] and $Bi_2Te(IO_3)O_5Cl$[141]) suggests that this type of compounds might also have promising mid-IR NLO prospect.

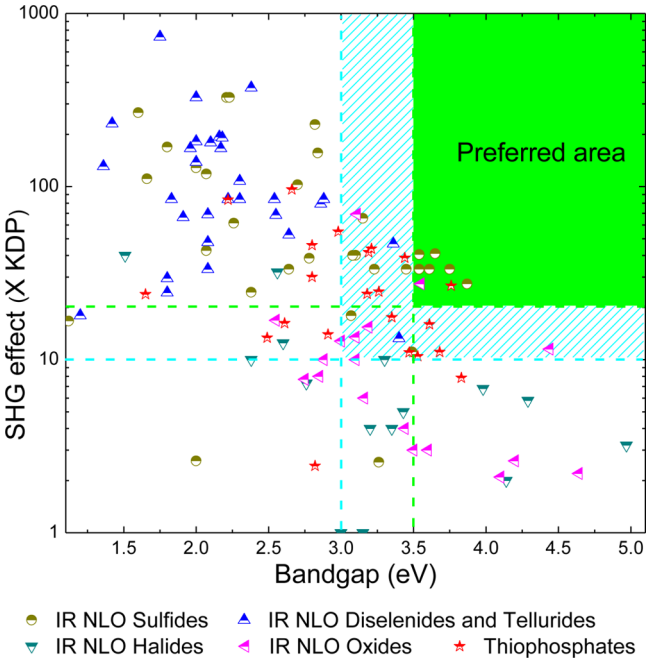

Figure 7. Distribution of E_g with respect to d_{ij} for numerous typical IR NLO crystals; the blue and green shaded regions represent the elementary (E_g > 3.0 eV and d_{ij} > 10 × KDP) and preferred (E_g > 3.5 eV and d_{ij} > 20 × KDP) conditions, respectively, for mid-IR NLO performance.

Compared with these types of IR NLO systems, metal thiophosphates exhibit comparable and even superior NLO performances (also see Figure 7). The strongest SHG effect is about 100 × KDP for $NaSbP_2S_6$, and the largest bandgap is about 3.8 eV for $K_3PS_4{\cdot}H_2O$. Furthermore, there are 11 thiophosphates, i.e., γ-Li_3PS_4, α-Na_3PS_4, P_4S_5, $KSbP_2S_6$, $Zn_3(PS_4)_2$, $LiZnPS_4$, $InPS_4$, $KInP_2S_7$, lt-$AlPS_4$, ht-$AlPS_4$, and $NaAlP_2S_6$, located in the blue area. This proportion (11 in 23 compounds studied in this work) is comparable to that in the other types of IR NLO materials, demonstrating the suitability of metal thiophosphates to be the good mid-IR NLO materials. In particular, the $LiZnPS_4$ crystal is predicted to exhibit both large bandgap and strong SHG effect (E_g = 3.76 eV and d_{ij} ~ 27 × KDP), might be the best mid-IR NLO candidate in the known metal thiophosphates. Meanwhile, this compound crystallizes in a uniaxial symmetry with moderate birefringence (~0.07). Therefore, $LiZnPS_4$ would have a very promising prospect for the mid-IR NLO laser generation. To further confirm our predictions, we select two compounds ($Zn_3(PS_4)_2$ and $LiZnPS_4$) in the 11 promising NLO thiophosphates and perform the primary experiments of synthesis and characterization (the experimental details are shown in the experimental section of the Supporting Information). The comparison between the calculated and experimental results is listed in Table 6. Clearly, the experimental results are in very good agreement with our predictions, which strongly demonstrate the suitability and

DOI: 10.1021/jacs.5b07920
J. Am. Chem. Soc. 2015, 137, 13049−13059

Table 6. Comparison between the Calculated and Experimental Results in $Zn_3(PS_4)_2$ and $LiZnPS_4$

		E_g (eV)	SHG effect
$Zn_3(PS_4)_2$	cal.	3.19	42 × KDP
	exp.	3.07	~53 × KDP
$LiZnPS_4$	cal.	3.76	27 × KDP
	exp.	3.44	~27 × KDP

accuracy of our computational methodology on the present study.

Finally, the importance of birefringence in the mid-IR NLO thiophosphates should be revisited. As an important optical property, birefringence is very crucial to produce the coherent generation through the SHG phase-matching technique. In fact, the phase-matching condition allows the relatively smaller birefringence in the mid-IR region than that in the visible and UV region, since the refractive-index dispersion is usually low in the long-wavelength region. For instance, a rather small optical birefringence ($\Delta n \sim 0.04$) may be enough to satisfy the elementary requirement of phase-matching condition in the mid-IR region, while the birefringence should be larger than 0.075 in the deep-UV region.[48] The shortest SHG output wavelengths λ_{SHG} from calculated birefringence values and refractive index dispersion curves (see Figure S3 and Figure S4 in the Supporting Information) show that most of the studied thiophosphates (except for Na_3PS_4) are able to generate the SHG output for the commonly used mid-IR laser input (2.09 μm). On the other hand, the too large birefringence ($\Delta n > 0.1$) would result in the destruction of strong coherent generation in crystal due to the self-focus and walk-off effects. Thus, a moderate range of birefringence from 0.04 to 0.10 would provide a suitable phase-matching condition for practical mid-IR NLO generation. In the studied thiophosphates the birefringence values of $Zn_3(PS_4)_2$, Li_3PS_4, $InPS_4$, P_4S_5 and ht-$AlPS_4$ (Δn = 0.035, 0.044, 0.048, 0.054 and 0.060, respectively) are comparable to the level of $AgGaS_2$ and $ZnGeP_2$ ($\Delta n \sim 0.045$), while the values of $LiZnPS_4$ and $KInP_2S_7$ (Δn = 0.073 and 0.078, respectively) are close to that of KBBF ($\Delta n \sim 0.077$). So they all satisfy the birefringence requirement in the mid-IR region very well. Moreover, as the uniaxial crystals, $InPS_4$, $Zn_3(PS_4)_2$, $LiZnPS_4$ and ht-$AlPS_4$ would be more convenient to realize the phase-matching condition. Although in practice the optical parametric oscillation (or difference frequency generation) is usually adopted to produce a mid/far-IR laser using NLO crystals, the above discussions still have instructive significance to the searching for good mid-IR NLO crystals.

4. CONCLUSION

With the purpose of searching for new mid-IR NLO materials that satisfy the conditions (I–IV), we highlight the family of metal thiophosphates as a very promising system of NLO materials with desirable properties for the mid-IR light generation. Totally 23 noncentrosymmetric *M*–*N*–P–S type thiophosphates with typically structural characteristics are systematically investigated using the first-principles simulations. The following was found: (i) Metal thiophosphates with isolated P–S groups possess wide E_g and strong d_{ij} but relatively small Δn, while γ-Li_3PS_4 has displayed the suitable mid-IR NLO properties. (ii) The introduction of SOJT or SALP *N* cations can significantly enhance the optical anisotropy so that both d_{ij} and Δn in crystal are enlarged. However, the electronic orbitals of the *N* cations occupy at the CBM and narrow the bandgap, thus these types of thiophosphates are some difficult to achieve the desirable balance between bandgap and SHG effect for mid-IR NLO generation. (iii) The introduction of *B*-site cations with relatively small covalent radius can effectively improve the optical anisotropy, while keeping the bandgaps wide enough. Hence the requirement for good mid-IR NLO performance would be easily satisfied in this type of thiophosphates. (iv) In all studied thiophosphates quite a few compounds exhibit the good capability for mid-IR coherent generation. Even the pure P–S binary compound P_4S_5 possesses the suitable mid-IR NLO properties. Remarkably, we predict that $LiZnPS_4$ has wide E_g, large d_{ij} and moderate Δn with uniaxial symmetry, and is a very promising mid-IR NLO material. Considering that the search for mid-IR NLO materials has not focused on the thiophosphate system yet, the present first-principles prediction and analysis, as confirmed by the primary experiments, would not only greatly promote the discovery of new mid-IR NLO materials, but also effectively provide a state-of-the-art way to understand the intrinsic mechanism for these important optoelectronic functional materials.

■ ASSOCIATED CONTENT

Supporting Information

The Supporting Information is available free of charge on the ACS Publications website at DOI: 10.1021/jacs.5b07920.

Tables S1–S4 and Figures S1–S4. Crystallographic data of the *M*–*N*–P–S type metal thiophosphates; Computational methods for SHG coefficients and real-space atom-cutting technique; Comparison of the experimental and calculated values of bandgaps E_g, SHG coefficients d_{ij} and birefringence Δn for several typically benchmark materials; The electronic densities distributed on the constituent atoms of Li_3PS_4, Na_3PS_4, and $K_3PS_4{\cdot}H_2O$; The DOS/PDOS, computed dispersion curves of refractive indices, the results of Mulliken bond populations and lengths of metal thiophosphates; The optical band gaps E_g (eV) and SHG effect d_{ij} (×KDP) for typical IR NLO crystals with different kinds of elemental compositions; The experimental methods of the synthesis and characterization for $Zn_3(PS_4)_2$ and $LiZnPS_4$; The shortest SHG output wavelengths λ_{SHG} with respect to the birefringence Δn. (PDF)

■ AUTHOR INFORMATION

Corresponding Author

*zslin@mail.ipc.ac.cn

Notes

The authors declare no competing financial interest.

■ ACKNOWLEDGMENTS

This work was supported by the National Natural Science Foundation of China under Grant Nos. 11174297 and China "863" project (No. 2015AA034203). The authors acknowledge the useful discussion from Zhuohong Yin.

■ REFERENCES

(1) Blake, G. A.; Laughlin, K. B.; Cohen, R. C.; Busarow, K. L.; Gwo, D. H.; Schmuttenmaer, C. A.; Steyert, D. W.; Saykally, R. J. *Rev. Sci. Instrum.* **1991**, *62*, 1693.

(2) Fischer, C.; Sigrist, M. W. *Solid-State Mid-Infrared Laser Sources*; Springer: Berlin, 2003; Vol. *89*, p 97.

(3) Smith, W. L. *Appl. Opt.* **1977**, *16*, 1798.

DOI: 10.1021/jacs.5b07920
J. Am. Chem. Soc. 2015, 137, 13049–13059

(4) Kato, K. *IEEE J. Quantum Electron.* **1991**, *27*, 1137.
(5) Chen, C. T.; Wu, B. C.; Jiang, A. D.; You, G. M. *Sci. Sin., Ser. B* **1985**, *28*, 235.
(6) Chen, C. T.; Wu, Y. C.; Jiang, A. D.; Wu, B. C.; You, G. M.; Li, R. K.; Lin, S. J. *J. Opt. Soc. Am. B* **1989**, *6*, 616.
(7) Boyd, G. D.; Nassau, K.; Miller, R. C.; Bond, W. L.; Savage, A. *Appl. Phys. Lett.* **1964**, *5*, 234.
(8) Duarte, F. J. *Tunable laser optics*; Elsevier Academic Press: New York, 2003.
(9) Jones-Bey, H. *Laser Focus World* **1998**, *34*, 127.
(10) Chen, C. T.; Wang, G. L.; Wang, X. Y.; Xu, Z. Y. *Appl. Phys. B: Lasers Opt.* **2009**, *97*, 9.
(11) Chung, I.; Kanatzidis, M. G. *Chem. Mater.* **2014**, *26*, 849.
(12) Kang, L.; Ramo, D. M.; Lin, Z. S.; Bristowe, P. D.; Qin, J. G.; Chen, C. T. *J. Mater. Chem. C* **2013**, *1*, 7363.
(13) Ra, H. S.; Ok, K. M.; Halasyamani, P. S. *J. Am. Chem. Soc.* **2003**, *125*, 7764.
(14) Kim, S.-H.; Yeon, J.; Halasyamani, P. S. *Chem. Mater.* **2009**, *21*, 5335.
(15) Wu, Q.; Meng, X.; Zhong, C.; Chen, X.; Qin, J. *J. Am. Chem. Soc.* **2014**, *136*, 5683.
(16) Okorogu, A. O.; Mirov, S. B.; Lee, W.; Crouthamel, D. I.; Jenkins, N.; Dergachev, A. Y.; Vodopyanov, K. L.; Badikov, V. V. *Opt. Commun.* **1998**, *155*, 307.
(17) Boyd, G. D.; Storz, F. G.; McFee, J. H.; Kasper, H. M. *IEEE J. Quantum Electron.* **1972**, *8*, 900.
(18) Bai, L.; Lin, Z. S.; Wang, Z. Z.; Chen, C. T.; Lee, M. H. *J. Chem. Phys.* **2004**, *120*, 8772.
(19) Boyd, G. D.; Buehler, E.; Storz, F. G. *Appl. Phys. Lett.* **1971**, *18*, 301.
(20) Jantz, W.; Koidl, P.; Wettling, W. *Appl. Phys. A: Solids Surf.* **1983**, *30*, 109.
(21) Kim, Y.; Seo, I. S.; Martin, S. W.; Baek, J.; Halasyamani, P. S.; Arumugam, N.; Steinfink, H. *Chem. Mater.* **2008**, *20*, 6048.
(22) Ni, Y.; Wu, H.; Wang, Z.; Mao, M.; Cheng, G.; Fei, H. *J. Cryst. Growth* **2009**, *311*, 1404.
(23) Isaenko, L.; Yelisseyev, A.; Lobanov, S.; Titov, A.; Petrov, V.; Zondy, J. J.; Krinitsin, P.; Merkulov, A.; Vedenyapin, V.; Smirnova, J. *Cryst. Res. Technol.* **2003**, *38*, 379.
(24) Patzmann, U.; Brockner, W. *Z. Naturforsch., A: Phys. Sci.* **1983**, *38*, 27.
(25) Toffoli, P.; Khodadad, P.; Rodier, N. *Acta Crystallogr., Sect. C: Cryst. Struct. Commun.* **1983**, *39*, 1485.
(26) Wu, Y.; Bensch, W. *J. Solid State Chem.* **2009**, *182*, 471.
(27) Joergens, S.; Mewis, A. *Solid State Sci.* **2007**, *9*, 213.
(28) Toffoli, P.; Rouland, J. C.; Khodadad, P.; Rodier, N. *Acta Crystallogr., Sect. C: Cryst. Struct. Commun.* **1985**, *41*, 645.
(29) Payne, M. C.; Teter, M. P.; Allan, D. C.; Arias, T. A.; Joannopoulos, J. D. *Rev. Mod. Phys.* **1992**, *64*, 1045.
(30) Kohn, W. *Rev. Mod. Phys.* **1999**, *71*, 1253.
(31) Clark, S. J.; Segall, M. D.; Pickard, C. J.; Hasnip, P. J.; Probert, M. J.; Refson, K.; Payne, M. C. *Z. Kristallogr. - Cryst. Mater.* **2005**, *220*, 567.
(32) Rappe, A. M.; Rabe, K. M.; Kaxiras, E.; Joannopoulos, J. D. *Phys. Rev. B: Condens. Matter Mater. Phys.* **1990**, *41*, 1227.
(33) Monkhorst, H. J.; Pack, J. D. *Phys. Rev. B* **1976**, *13*, 5188.
(34) Rashkeev, S. N.; Lambrecht, W. R. L.; Segall, B. *Phys. Rev. B: Condens. Matter Mater. Phys.* **1998**, *57*, 3905.
(35) Lin, J.; Lee, M. H.; Liu, Z. P.; Chen, C. T.; Pickard, C. J. *Phys. Rev. B: Condens. Matter Mater. Phys.* **1999**, *60*, 13380.
(36) Kurtz, S. K.; Perry, T. T. *J. Appl. Phys.* **1968**, *39*, 3798.
(37) Asahi, R.; Mannstadt, W.; Freeman, A. J. *Phys. Rev. B: Condens. Matter Mater. Phys.* **1999**, *59*, 7486.
(38) Bera, T. K.; Jang, J. I.; Song, J. H.; Malliakas, C. D.; Freeman, A. J.; Ketterson, J. B.; Kanatzidis, M. G. *J. Am. Chem. Soc.* **2010**, *132*, 3484.
(39) Gillen, R.; Robertson, J. *Phys. Rev. B: Condens. Matter Mater. Phys.* **2011**, DOI: 10.1103/PhysRevB.84.035125.
(40) Ceperley, D. M.; Alder, B. J. *Phys. Rev. Lett.* **1980**, *45*, 566.
(41) Godby, R. W.; Schluter, M.; Sham, L. J. *Phys. Rev. B: Condens. Matter Mater. Phys.* **1988**, *37*, 10159.
(42) Lin, Z. S.; Jiang, X. X.; Kang, L.; Gong, P. F.; Luo, S. Y.; Lee, M. H. *J. Phys. D: Appl. Phys.* **2014**, DOI: 10.1088/0022-3727/47/25/253001.
(43) Lin, X.; Zhang, G.; Ye, N. *Cryst. Growth Des.* **2009**, *9*, 1186.
(44) Yao, J. Y.; Mei, D. J.; Bai, L.; Lin, Z. S.; Yin, W. L.; Fu, P. Z.; Wu, Y. C. *Inorg. Chem.* **2010**, *49*, 9212.
(45) Homma, K.; Yonemura, M.; Kobayashi, T.; Nagao, M.; Hirayama, M.; Kanno, R. *Solid State Ionics* **2011**, *182*, 53.
(46) Jansen, M.; Henseler, U. *J. Solid State Chem.* **1992**, *99*, 110.
(47) Volk, K.; Schafer, H. *Z. Naturforsch., B: J. Chem. Sci.* **1979**, *34*, 1337.
(48) Chen, C.; Lin, Z.; Wang, Z. *Appl. Phys. B: Lasers Opt.* **2005**, *80*, 1.
(49) Vos, A.; Olthof, R.; Vanbolhu, F.; Botterwe, R. *Acta Crystallogr.* **1965**, *19*, 864.
(50) Bera, T. K.; Jang, J. I.; Ketterson, J. B.; Kanatzidis, M. G. *J. Am. Chem. Soc.* **2009**, *131*, 75.
(51) Pell, M. A.; Vajenine, G. V. M; Ibers, J. A. *J. Am. Chem. Soc.* **1997**, *119*, 5186.
(52) Zhukov, V.; Boucher, F.; Alemany, P.; Evain, M.; Alvarez, S. *Inorg. Chem.* **1995**, *34*, 1159.
(53) Lee, S.; Colombet, P.; Ouvrard, G.; Brec, R. *Inorg. Chem.* **1988**, *27*, 1291.
(54) Reinen, D.; Friebel, C. *Inorg. Chem.* **1984**, *23*, 792.
(55) Pearson, R. G. *Proc. Natl. Acad. Sci. U. S. A.* **1975**, *72*, 2104.
(56) Pearson, R. G. *J. Am. Chem. Soc.* **1969**, *91*, 4947.
(57) Pearson, R. G. *J. Mol. Struct.: THEOCHEM* **1983**, *12*, 25.
(58) Jandali, M. Z.; Eulenberger, G.; Hahn, H. *Z. Anorg. Allg. Chem.* **1980**, *470*, 39.
(59) Boucher, F.; Evain, M.; Brec, R. *Acta Crystallogr., Sect. B: Struct. Sci.* **1995**, *51*, 952.
(60) Mulliken, R. S. *J. Chem. Phys.* **1955**, *23*, 1833.
(61) Post, E.; Kramer, V. *Mater. Res. Bull.* **1984**, *19*, 1607.
(62) Aitken, J. A.; Kanatzidis, M. G. *Inorg. Chem.* **2001**, *40*, 2938.
(63) Yao, J. Y.; Ibers, J. A. *Acta Crystallogr., Sect. E: Struct. Rep. Online* **2004**, *60*, I108.
(64) Gave, M. A.; Weliky, D. P.; Kanatzidis, M. G. *Inorg. Chem.* **2007**, *46*, 11063.
(65) Manriquez, V.; Galdamez, A.; Ruiz-Leon, D. *Mater. Res. Bull.* **2006**, *41*, 1337.
(66) Manriquez, V.; Galdamez, A.; Leon, D. R.; Garland, M. T. *Z. Kristallogr. - New Cryst. Struct.* **2003**, *218*, 403.
(67) Manriquez, V.; Galdamez, A.; Leon, D. R.; Garland, M. T.; Jimenez, M. *Z. Kristallogr. - New Cryst. Struct.* **2003**, *218*, 151.
(68) Becker, R.; Brockner, W.; Eisenmann, B. *Z. Naturforsch., A: Phys. Sci.* **1987**, *42*, 1309.
(69) Gave, M. A.; Malliakas, C. D.; Weliky, D. P.; Kanatzidis, M. G. *Inorg. Chem.* **2007**, *46*, 3632.
(70) Jorgens, S.; Johrendt, D.; Mewis, A. *Z. Anorg. Allg. Chem.* **2002**, *628*, 1765.
(71) Diehl, R.; Carpentier, C. D. *Acta Crystallogr., Sect. B: Struct. Crystallogr. Cryst. Chem.* **1978**, *34*, 1097.
(72) Kopnin, E.; Coste, S.; Jobic, S.; Evain, M.; Brec, R. *Mater. Res. Bull.* **2000**, *35*, 1401.
(73) Kuhn, A.; Eger, R.; Ganter, P.; Duppel, V.; Nuss, J.; Lotsch, B. V. *Z. Anorg. Allg. Chem.* **2014**, *640*, 2663.
(74) Kuhn, A.; Eger, R.; Nuss, J.; Lotsch, B. V. *Z. Anorg. Allg. Chem.* **2013**, *639*, 1087.
(75) Kang, L.; Lin, Z. S.; Qin, J. G.; Chen, C. T. *Sci. Rep.* **2013**, *3*, 1366.
(76) Dovgii, Y. O.; Kityk, I. V. *Phys. Status Solidi B* **1991**, *166*, 395.
(77) Levine, B. F.; Bethea, C. G.; Kasper, H. M.; Thiel, F. A. *IEEE J. Quantum Electron.* **1976**, *12*, 367.
(78) Isaenko, L.; Vasilyeva, I.; Merkulov, A.; Yelisseyev, A.; Lobanov, S. *J. Cryst. Growth* **2005**, *275*, 217.
(79) Yin, W.; Feng, K.; Hao, W.; Yao, J.; Wu, Y. *Inorg. Chem.* **2012**, *51*, 5839.
(80) Lekse, J. W.; Moreau, M. A.; McNerny, K. L.; Yeon, J.; Halasyamani, P. S.; Aitken, J. A. *Inorg. Chem.* **2009**, *48*, 7516.

DOI: 10.1021/jacs.5b07920
J. Am. Chem. Soc. 2015, 137, 13049−13059

(81) Brant, J. A.; Clark, D. J.; Kim, Y. S.; Jang, J. I.; Weiland, A.; Aitken, J. A. *Inorg. Chem.* **2015**, *54*, 2809.
(82) Yin, W. L.; Feng, K.; He, R.; Mei, D. J.; Lin, Z. S.; Yao, J. Y.; Wu, Y. C. *Dalton Trans.* **2012**, *41*, 5653.
(83) Luo, Z. Z.; Lin, C. S.; Cui, H. H.; Zhang, W. L.; Zhang, H.; He, Z. Z.; Cheng, W. D. *Chem. Mater.* **2014**, *26*, 2743.
(84) Lin, Z. H.; Li, C.; Kang, L.; Lin, Z. S.; Yao, J. Y.; Wu, Y. C. *Dalton Trans.* **2015**, *44*, 7404.
(85) Li, X.; Kang, L.; Li, C.; Lin, Z.; Yao, J.; Wu, Y. *J. Mater. Chem. C* **2015**, *3*, 3060.
(86) Feng, K.; Kang, L.; Lin, Z. S.; Yao, J. Y.; Wu, Y. C. *J. Mater. Chem. C* **2014**, *2*, 4590.
(87) Bera, T. K.; Song, J. H.; Freeman, A. J.; Jang, J. I.; Ketterson, J. B.; Kanatzidis, M. G. *Angew. Chem., Int. Ed.* **2008**, *47*, 7828.
(88) Chen, M. C.; Li, L. H.; Chen, Y. B.; Chen, L. *J. Am. Chem. Soc.* **2011**, *133*, 4617.
(89) Zhao, H.-J.; Zhang, Y.-F.; Chen, L. *J. Am. Chem. Soc.* **2012**, *134*, 1993.
(90) Geng, L.; Cheng, W.-D.; Lin, C.-S.; Zhang, W.-L.; Zhang, H.; He, Z.-Z. *Inorg. Chem.* **2011**, *50*, 5679.
(91) Reshak, A. H.; Azam, S. *Opt. Mater.* **2014**, *37*, 97.
(92) Kuo, S. M.; Chang, Y. M.; Chung, I.; Jang, J. I.; Her, B. H.; Yang, S. H.; Ketterson, J. B.; Kanatzidis, M. G.; Hsu, K. F. *Chem. Mater.* **2013**, *25*, 2427.
(93) Durichen, P.; Bensch, W. *Acta Crystallogr., Sect. C: Cryst. Struct. Commun.* **1998**, *54*, 706.
(94) Luo, Z. Z.; Lin, C. S.; Zhang, W. L.; Zhang, H.; He, Z. Z.; Cheng, W. D. *Chem. Mater.* **2014**, *26*, 1093.
(95) Chen, M. C.; Wu, L. M.; Lin, H.; Zhou, L. J.; Chen, L. *J. Am. Chem. Soc.* **2012**, *134*, 6058.
(96) Mei, D. J.; Gong, P. F.; Lin, Z. S.; Feng, K.; Yao, J. Y.; Huang, F. Q.; Wu, Y. C. *CrystEngComm* **2014**, *16*, 6836.
(97) Abdullae, Gb; Kulevski, La; Smirnov, V. V.; Salaev, E. Y.; Savelev, A. D.; Prokhoro, Am *JETP Lett.* **1972**, *16*, 90.
(98) Mei, D. J.; Yin, W. L.; Feng, K.; Lin, Z. S.; Bai, L.; Yao, J. Y.; Wu, Y. C. *Inorg. Chem.* **2012**, *51*, 1035.
(99) Zhang, J. H.; Clark, D. J.; Brant, J. A.; Sinagra, C. W.; Kim, Y. S.; Jang, J. I.; Aitken, J. A. *Dalton Trans.* **2015**, *44*, 11212.
(100) Mei, D.; Yin, W.; Bai, L.; Lin, Z.; Yao, J.; Fu, P.; Wu, Y. *Dalton Trans.* **2011**, *40*, 3610.
(101) Luo, Z. Z.; Lin, C. S.; Cui, H. H.; Zhang, W. L.; Zhang, H.; Chen, H.; He, Z. Z.; Cheng, W. D. *Chem. Mater.* **2015**, *27*, 914.
(102) Yu, P.; Zhou, L. J.; Chen, L. *J. Am. Chem. Soc.* **2012**, *134*, 2227.
(103) Chung, I.; Malliakas, C. D.; Jang, J. I.; Canlas, C. G.; Weliky, D. P.; Kanatzidis, M. G. *J. Am. Chem. Soc.* **2007**, *129*, 14996.
(104) Banerjee, S.; Malliakas, C. D.; Jang, J. I.; Ketterson, J. B.; Kanatzidis, M. G. *J. Am. Chem. Soc.* **2008**, *130*, 12270.
(105) Chung, I.; Kim, M. G.; Jang, J. I.; He, J. Q.; Ketterson, J. B.; Kanatzidis, M. G. *Angew. Chem., Int. Ed.* **2011**, *50*, 10867.
(106) Haynes, A. S.; Saouma, F. O.; Otieno, C. O.; Clark, D. J.; Shoemaker, D. P.; Jang, J. I.; Kanatzidis, M. G. *Chem. Mater.* **2015**, *27*, 1837.
(107) Chung, I.; Song, J. H.; Jang, J. I.; Freeman, A. J.; Kanatzidis, M. G. *J. Solid State Chem.* **2012**, *195*, 161.
(108) Morris, C. D.; Chung, I.; Park, S.; Harrison, C. M.; Clark, D. J.; Jang, J. I.; Kanatzidis, M. G. *J. Am. Chem. Soc.* **2012**, *134*, 20733.
(109) Syrigos, J. C.; Clark, D. J.; Saouma, F. O.; Clarke, S. M.; Fang, L.; Jang, J. I.; Kanatzidis, M. G. *Chem. Mater.* **2015**, *27*, 255.
(110) Chung, I.; Song, J. H.; Jang, J. I.; Freeman, A. J.; Ketterson, J. B.; Kanatzidis, M. G. *J. Am. Chem. Soc.* **2009**, *131*, 2647.
(111) Chen, Y.-K.; Chen, M.-C.; Zhou, L.-J.; Chen, L.; Wu, L.-M. *Inorg. Chem.* **2013**, *52*, 8334.
(112) Zhang, J.; Su, N. B.; Yang, C. L.; Qin, J. G.; Ye, N.; Wu, B. C.; Chen, C. T. In *Electro-Optic and Second Harmonic Generation Materials, Devices, and Applications II*; Chen, C., Ed.; SPIE: Bellingham, WA, 1998; Vol. *3556*, p 1.
(113) Tang, L. C.; Huang, J. Y.; Chang, C. S.; Lee, M. H.; Liu, L. Q. *J. Phys.: Condens. Matter* **2005**, *17*, 7275.
(114) Tang, L. C.; Chang, C. S.; Huang, J. Y. *J. Phys.: Condens. Matter* **2000**, *12*, 9129.
(115) Stoumpos, C. C.; Frazer, L.; Clark, D. J.; Kim, Y. S.; Rhim, S. H.; Freeman, A. J.; Ketterson, J. B.; Jang, J. I.; Kanatzidis, M. G. *J. Am. Chem. Soc.* **2015**, *137*, 6804.
(116) Ren, P.; Qin, J. G.; Chen, C. T. *Inorg. Chem.* **2003**, *42*, 8.
(117) Lv, S. W.; Wu, Q.; Meng, X. G.; Kang, L.; Zhong, C.; Lin, Z. S.; Hu, Z. G.; Chen, X. G.; Qin, J. G. *J. Mater. Chem. C* **2014**, *2*, 6796.
(118) Zhang, G.; Qin, J. G.; Liu, T.; Zhu, T. X.; Fu, P. Z.; Wu, Y. C.; Chen, C. T. *Cryst. Growth Des.* **2008**, *8*, 2946.
(119) Zhang, G.; Qin, J. G.; Liu, T.; Li, Y. J.; Wu, Y. C.; Chen, C. T. *Appl. Phys. Lett.* **2009**, *95*, 95.
(120) Zhang, G.; Liu, T.; Zhu, T. X.; Qin, J. G.; Wu, Y. C.; Chen, C. T. *Opt. Mater.* **2008**, *31*, 110.
(121) Liu, T.; Qin, J.; Zhang, G.; Zhu, T.; Niu, F.; Wu, Y.; Chen, C. *Appl. Phys. Lett.* **2008**, DOI: 10.1063/1.2969059.
(122) Ferrier, A.; Velazquez, M.; Portier, X.; Doualan, J. L.; Moncorge, R. *J. Cryst. Growth* **2006**, *289*, 357.
(123) Bergman, J. G.; Crane, G. R. *J. Chem. Phys.* **1974**, *60*, 2470.
(124) Li, Y. J.; Wang, M.; Zhu, T. X.; Meng, X. G.; Zhong, C.; Chen, X. G.; Qin, J. G. *Dalton Trans.* **2012**, *41*, 763.
(125) Huang, Y.; Meng, X. G.; Kang, L.; Li, Y. J.; Zhong, C.; Lin, Z. S.; Chen, X. G.; Qin, J. G. *CrystEngComm* **2013**, *15*, 4196.
(126) Zhang, G.; Li, Y. J.; Jiang, K.; Zeng, H. Y.; Liu, T.; Chen, X. G.; Qin, J. G.; Lin, Z. S.; Fu, P. Z.; Wu, Y. C.; Chen, C. T. *J. Am. Chem. Soc.* **2012**, *134*, 14818.
(127) Sun, C.-F.; Hu, C.-L.; Xu, X.; Ling, J.-B.; Hu, T.; Kong, F.; Long, X.-F.; Mao, J.-G. *J. Am. Chem. Soc.* **2009**, *131*, 9486.
(128) Nguyen, S. D.; Yeon, J.; Kim, S. H.; Halasyamani, P. S. *J. Am. Chem. Soc.* **2011**, *133*, 12422.
(129) Chang, H. Y.; Kim, S. H.; Ok, K. M.; Halasyamani, P. S. *J. Am. Chem. Soc.* **2009**, *131*, 6865.
(130) Zhou, Y.; Hu, C.-L.; Hu, T.; Kong, F.; Mao, J.-G. *Dalton Trans.* **2009**, 5747.
(131) Chi, E. O.; Ok, K. M.; Porter, Y.; Halasyamani, P. S. *Chem. Mater.* **2006**, *18*, 2070.
(132) Zhang, J. J.; Tao, X. T.; Sun, Y. X.; Zhang, Z. H.; Zhang, C. Q.; Gao, Z. L.; Xia, H. B.; Xia, S. Q. *Cryst. Growth Des.* **2011**, *11*, 1863.
(133) Sykora, R. E.; Ok, K. M.; Halasyamani, P. S.; Albrecht-Schmitt, T. E. *J. Am. Chem. Soc.* **2002**, *124*, 1951.
(134) Zhao, S. G.; Luo, J. H.; Zhou, P.; Zhang, S. Q.; Sun, Z. H.; Hong, M. C. *RSC Adv.* **2013**, *3*, 14000.
(135) Kim, Y. H.; Lee, D. W.; Ok, K. M. *Inorg. Chem.* **2014**, *53*, 5240.
(136) Kong, F.; Huang, S. P.; Sun, Z. M.; Mao, J. G.; Cheng, W. D. *J. Am. Chem. Soc.* **2006**, *128*, 7750.
(137) Huang, Y.-Z.; Wu, L.-M.; Wu, X.-T.; Li, L.-H.; Chen, L.; Zhang, Y.-F. *J. Am. Chem. Soc.* **2010**, *132*, 12788.
(138) Zhang, W. L.; Cheng, W. D.; Zhang, H.; Geng, L.; Lin, C. S.; He, Z. Z. *J. Am. Chem. Soc.* **2010**, *132*, 1508.
(139) Eckardt, R. C.; Masuda, H.; Fan, Y. X.; Byer, R. L. *IEEE J. Quantum Electron.* **1990**, *26*, 922.
(140) Zhang, H.; Zhang, M.; Pan, S. L.; Dong, X. Y.; Yang, Z. H.; Hou, X. L.; Wang, Z.; Chang, K. B.; Poeppelmeier, K. R. *J. Am. Chem. Soc.* **2015**, *137*, 8360.
(141) Geng, L.; Meng, C. Y.; Lu, H. Y.; Luo, Z. Z.; Lin, C. S.; Cheng, W. D. *Dalton Trans.* **2015**, *44*, 2469.

DOI: 10.1021/jacs.5b07920
J. Am. Chem. Soc. 2015, 137, 13049−13059